PhenomPv2 - Technical notes for the LAL implementation

LIGO Document T1500602-v4

Alejandro Bohé[1], Mark Hannam[2], Sascha Husa[3], Frank Ohme[2], Michael Pürrer[1], and Patricia Schmidt[4,5]

[1] *Max Planck Institute for Gravitational Physics (Albert Einstein Institute), Am Mühlenberg 1, Potsdam 14476, Germany*
[2] *School of Physics and Astronomy, Cardiff University, Queens Building, CF24 3AA, Cardiff, United Kingdom*
[3] *Departament de Física, Universitat de les Illes Balears, Crta. Valldemossa km 7.5, E-07122 Palma, Spain*
[4] *LIGO Laboratory, California Institute of Technology, MS 100-36, Pasadena, California91125, USA*
[5] *Theoretical Astrophysics 350-17, California Institute of Technology, Pasadena, CA 91125, USA*

20 May 2016

Abstract

These notes describe the lal implementation of the PhenomPv2 model. In particular, they will cover

- Conventions
- A short introduction to the model: definition of the main ingredients
- From PhenomD to PhenomP: twisting up in the frequency domain
- Derivation of the expressions for the Euler angles
- Transformation function from lal parameters (input of ChooseFD...) to the intrinsic parameters of the model
- Final spin

1 Notation and conventions

1.1 Key References

The PhenomP model has been presented in the paper [6], the review wiki pages can be found at [1]. This model is based on the non-precessing PhenomD model, presented in [7, 8] (which we will refer to as papers I and II below), for the internal review see [2].

1.2 Fourier conventions

We use the following Fourier transform convention for the FT $\tilde{h}(f)$ of a function $h(t)$

$$FT[h](f) \equiv \tilde{h}(f) = \int_{-\infty}^{+\infty} e^{-2\pi i f t} f(t)\,\mathrm{d}t \tag{1}$$

which is the usual convention in LAL. This is also the same convention as in the PhenomD papers (see Eq (2.4) of Paper I).

Note that in PhenomD (see Eq (2.1) of Paper I), which models only the dominant $(\ell, |m|) = (2, 2)$ modes of aligned spin systems, the time domain phase of the (2,2) mode is defined with the convention

$$h^D_{2,2}(t) = A_D(t) e^{-i\phi_D(t)} \tag{2}$$

with $\dot{\phi}_D < 0$ so that the $(2, 2)$ mode has most of its power in the positive frequency range ($f > 0$) (in the context of an SPA approximation, *all* the power would be in positive frequencies). Correspondingly $h^D_{2,-2}(t) = \left(h^D_{2,2}(t)\right)^*$ has its power in the negative frequency range.

In the Fourier domain, the convention for PhenomD is (see Eq (7) of Paper II)

$$\tilde{h}^D_{2,2}(f) = A_D(f) e^{-i\phi_D(f)}$$

which is valid for $f > 0$ (and $\tilde{h}^D_{2,2}(f) = 0$ for $f < 0$). Correspondingly,

$$\tilde{h}^D_{2,-2}(f) = \left(\tilde{h}^D_{2,2}(-f)\right)^* = A_D(-f)e^{i\phi_D(-f)}$$

for $f < 0$ and is zero for positive frequencies.

However, this is a different convention from for instance Arun et al. [3] which is what is used for SpinTaylorTx in LAL since there the (2,2) mode is of the form $h_{2,2}(t) = A(t)e^{-i\phi(t)}$ with $\dot{\phi} > 0$ (see for instance their Eq (4.16)). This means that between PhenomD and SpinTaylor, there is a conjugation at the level of the modes, which at the level of the full waveform $h_+ - ih_\times$ corresponds to a redefinition of the polarizations (changing the sign of $h_\times$, i.e. a global conjugation) *and* and a redefinition $\varphi \to -\varphi$ (see Fig. 1 for the definition of the azimuthal angle φ). In order to stick to the convention of SpinTaylorTx, we therefore change the convention of PhenomD by conjugating the modes, which amounts to exchanging the $(2, 2)$ and $(2, -2)$ modes. We therefore redefine the time domain phase so that (2) holds but with

$$\dot{\phi}_D(t) > 0 \tag{3}$$

and in the Fourier domain

$$\tilde{h}^D_{2,-2}(f) = A_D(f)e^{-i\phi_D(f)} \tag{4}$$

for $f > 0$ and $\tilde{h}^D_{2,2}(f) = \left(\tilde{h}^D_{2,-2}(-f)\right)^* = A_D(-f)e^{i\phi_D(-f)}$ for $f < 0$. The functions `IMRPhenDPhase` and `IMRPhenDAmplitude` compute the quantities $\phi_D(f)$ and $\hat{A}_D(f)$, where

$$A_D(f) = a_0\,\hat{A}_D(f), \qquad a_0 = 2\sqrt{\frac{5}{64 LAL\_PI}}\,\frac{M^2 \times LAL\_MRSUN\_SI \times LAL\_MTSUN\_SI}{distance}, \tag{5}$$

using `LAL` variable names for the constant π and the distance and solar mass converted to length and time in SI units, and the total binary mass M in units of solar masses, and the numerical pre-factor derives from the normalization of the $Y_{2|2|}$ spin-weighted spherical harmonic.

2 Brief intro to the model

The idea at the core of the model is the fact that a precessing waveform can be approximated by appropriately rotating a non precessing waveform [12].

More precisely, in a suitable co-precessing (non inertial) frame which tracks the precession of the orbital plane [13] and that we will define below, the waveform is close to the waveform that would be produced by an aligned spin system (with the same masses and spin projections along the normal to the orbital plane) in the usual inertial frame associated to it [13, 5, 12]. Therefore, one can approximately model precessing waveforms by combining models for aligned spin waveforms (we use PhenomD) and for the rotation that tracks the precession of the orbital plane (this will be described in Sec. 3).

Our conventions for the different frames and angles closely follow those of Arun et al [3] (see in particular Fig 1 there) which is what is also used for SpinTaylorTx in LAL. We briefly summarize the key definitions below to make this document self contained.

- We consider an inertial frame whose z axis is aligned with the direction of the total angular momentum $\hat{\mathbf{J}}$ at some reference frequency $f_{\rm ref}$. The triad used to define the two polarizations is the same as in Arun et al. (see fig 1)
- The spherical angles (β, α) parametrize the direction of the Newtonian orbital angular momentum $\hat{\mathbf{L}}_\mathbf{N}$ in the inertial frame. Note that in Arun et al, β is called ι but in LAL this usually denotes the angle between $\hat{\mathbf{L}}_\mathbf{N}$ and the line of sight $\hat{\mathbf{N}}$ (and is often called inclination). We use the spherical angles (θ, φ) to parametrize the direction of $\hat{\mathbf{N}}$.

  Some arbitrary choice is made for the x and y axes (one can impose for instance that the line of sight is in the xz plane or that at $f_{\rm ref}$, the vector $\hat{\mathbf{L}}_\mathbf{N}$ is in the xz plane. Of course physically, only the difference $\alpha - \varphi$ matters. [In the code, we chose to set $\varphi = 0$].
- We now define our co-precessing frame. Since we choose to track the precession of the orbital plane, we define $\hat{\mathbf{z}}' = \hat{\mathbf{L}}_\mathbf{N}$. We still have to fix the rotation freedom around $\hat{\mathbf{L}}_\mathbf{N}$ which we can do by choosing $\hat{\mathbf{x}}'$. Equivalently, we could have defined our co-precessing frame by specifying the (time dependent) rotation between the two triads $(\hat{\mathbf{x}}, \hat{\mathbf{y}}, \hat{\mathbf{z}})$ and $(\hat{\mathbf{x}}', \hat{\mathbf{y}}', \hat{\mathbf{z}}')$. In terms of the three Euler angles needed to parametrize this rotation, the choice $\hat{\mathbf{z}}' = \hat{\mathbf{L}}_\mathbf{N}$ constrains the first two Euler angles to be α and ι **[of course, we need to give a ref for the convention we adopt for the Euler angles]**. We define the third angle through the usual relation

  $$\dot{\epsilon} = \dot{\alpha}\cos\beta \tag{6}$$

  which corresponds to $\hat{\mathbf{x}}' = \hat{\mathbf{x}}_L$ in the notation of Arun et al.[3]. Note that all three Euler angles vary on the precessional timescale.

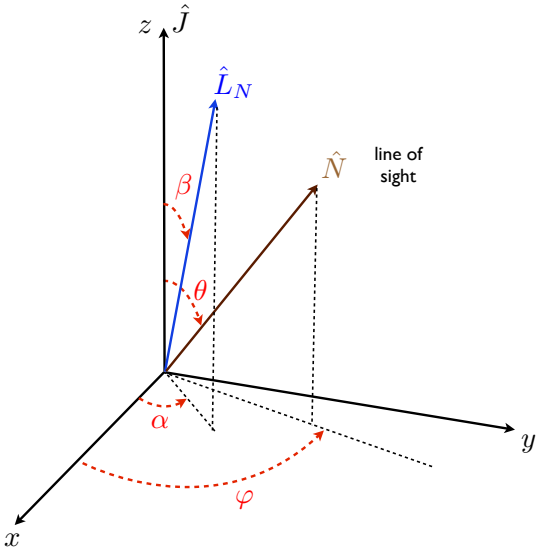

Figure 1: The "unit" Newtonian orbital angular momentum $\boldsymbol{\ell}$ is parametrized by its spherical angles (β, α) in a frame where $\hat{\mathbf{z}} = \hat{\mathbf{J}}$. The line of sight is parametrized by (θ, φ)

- In the context of PhenomP, the waveform in this co-precessing frame is approximated by an aligned spin waveform computed using the PhenomD model. In particular, this implies the following approximations for the waveform in the co-precessing frame (on top of the fact that the $(2,2)$ mode is only approximately that of an aligned spin waveform),
  - only the $(\ell, |m|) = (2,2)$ modes are considered (this approximation degrades as the mass ratio increases, but it is the usual approximation in the context of aligned spin waveforms)
  - we assume the usual symmetry for the time domain modes $h_{2,2} = h^*_{2,-2}$
- With these definitions, the modes of the waveform in the inertial frame are related to those of the waveform in the co-precessing frame by the rotation

$$h^{\rm inertial}_{\ell m}(t) = e^{-im\alpha} \sum_{m'} e^{im'\epsilon} d^{\ell}_{m',m}(-\beta) h^{\rm co-prec}_{\ell,m'}(t), \tag{7}$$

We use the following convention for the Wigner matrices

$$d^{l}_{m',m}(\beta) = \sum (-1)^{k+m'-m} \frac{\sqrt{(l+m)!(l-m)!(l+m')!(l-m')!}}{(l+m-k)!(l-m-k)!k!(m'-m+k)!} \left(\cos\frac{\beta}{2}\right)^{2l-2k-m'+m} \left(\sin\frac{\beta}{2}\right)^{2k+m'-m} \tag{8}$$

(the sum is over all values of k for which all the arguments of the factorials are positive).

Specializing to our case where the co-precessing waveform is taken to be PhenomD (denoted with a superscript "D") which has only $(2,|2|)$ modes, and replacing the "inertial" superscript by "P" for PhenomP, we obtain that PhenomP describes only the $\ell = 2$ modes in the inertial frame, for which we have

$$h^{P}_{2m}(t) = e^{-im\alpha} \sum_{|m'|=2} e^{im'\epsilon} d^{2}_{m',m}(-\beta) h^{D}_{2,m'}(t), \tag{9}$$

In section 3, we derive the corresponding "twisting up" formula in the Fourier domain (using an SPA approximation to perform the Fourier transform). Then in section 4, we outline the derivation of analytic expressions (using a PN approximation) for our Euler angles as a function of frequency.

3 Twisting up in the frequency domain

We start from the twisting formula in the time domain

$$h^{\rm P}_{2m}(t) = e^{-im\alpha(t)} \left[h^{\rm D}_{22}(t) d^{2}_{2,m}(-\beta(t)) e^{2i\epsilon(t)} + h^{\rm D}_{2,-2}(t) d^{2}_{-2,m}(-\beta(t)) e^{-2i\epsilon(t)} \right] \tag{10}$$

and apply the SPA separately to each part, using the fact that the timescale of variation of the angles is the precession timescale, which is much longer than the orbital timescale so we can treat all the angle-dependent

factors as a slowly varying amplitude.

Let us look for instance at the first term $\kappa_+(t) = h^{\rm D}_{22}(t) d^2_{2,m}(-\beta(t)) e^{2i\epsilon(t)} e^{-im\alpha(t)} = A_+(t) e^{-i\phi_D(t)}$ with $A_+(t) = A_D(t) d^2_{2,m}(-\beta(t)) e^{2i\epsilon(t)} e^{-im\alpha(t)}$ varying on the precession timescale (as opposed to the shorter orbital timescale on which ϕ_D varies). Then within the SPA, we look for $t_+(f)$ which satisfies

$$\dot{\phi}_D(t_+(f)) = -2\pi f \tag{11}$$

(this has solutions only if $f < 0$ with our conventions) and we have

$$\tilde{\kappa}_+(f) = \left\{ \begin{array}{cc} 0 & f > 0 \\ d^2_{2,m}(-\beta(t_+(f))) e^{2i\epsilon(t_+(f))} e^{-im\alpha(t_+(f))} \tilde{h}^{\rm D}_{22}(f) & f < 0 \end{array} \right. \tag{12}$$

In the expression above, the angles have to be evaluated at $t = t_+(f)$. However, our PN expressions for the angles are naturally expressed in terms of the orbital frequency ω (see next section) so in fact we need to evaluate them at $\omega(t_+(f))$. But the time evolution of ω only depends on the components of the spins perpendicular to the orbital plane (at least at the spin-orbit level...) so that $2\omega(t)$ is actually equal to $\dot{\phi}_D(t)$ (the important point is that the phase entering in (11) is that of the (2,2) mode of PhenomD which has the same ortho spins as the configuration that we are trying to model) and therefore $\omega(t_+(f)) = -\pi f$. The same treatment for the second term shows that it only contributes for $f > 0$.

Finally, given PN expressions for the angles as functions of ω (i.e. $\beta(\omega)$, $\alpha(\omega)$, and $\epsilon(\omega)$) and a frequency domain expression for the 22 mode of PhenomD, we obtain our twisted up PhenomP modes in the frequency domain

$$\tilde{h}^{\rm P}_{2m}(f) = \left\{ \begin{array}{cc} d^2_{-2,m}\big(-\beta(\pi f)\big) e^{i\left(-2\epsilon(\pi f) - m\alpha(\pi f)\right)} \left(\tilde{h}^{\rm D}_{22}(-f)\right)^* & f > 0 \\ d^2_{2,m}\big(-\beta(-\pi f)\big) e^{i\left(2\epsilon(-\pi f) - m\alpha(-\pi f)\right)} \tilde{h}^{\rm D}_{22}(f) & f < 0 \end{array} \right. \tag{13}$$

Note that because $d^2_{-2,-m} = (-1)^m d^2_{2,m}$, we have $\tilde{h}^{\rm P}_{2,m}(-f) = \left(\tilde{h}^{\rm P}_{2,-m}(f)\right)^* (-1)^m$.

Now that we have expressions for the modes, we can reconstruct the two polarizations from

$$\tilde{h}(\theta,\phi,f) = \tilde{h}_+(\theta,\phi,f) - i\tilde{h}_\times(\theta,\phi,f) = \sum_{l,m} {}^{-2}Y_{l,m}(\theta,\phi)\tilde{h}_{2,m}(f) \tag{14}$$

Starting with the + polarization,

$$\widetilde{h_+}(\theta,\varphi,f) = ({\rm FT}[h_+(\theta,\varphi,t)]) = ({\rm FT}[{\rm Re}\, h(\theta,\varphi,t)])(f) \tag{15}$$

This is the Fourier transform of a real function so we have $\widetilde{h_+}(f) = \left(\widetilde{h_+}(-f)\right)^*$ and therefore, we only need to obtain an expression for positive frequencies (for instance).

For $f > 0$, we have,

$$\begin{aligned}
\widetilde{h_+}(\theta,\varphi,f) &= ({\rm FT}[{\rm Re}\, h(\theta,\varphi,t)])(f) = \left({\rm FT}\left[\frac{1}{2}(h(\theta,\varphi,t) + h(\theta,\varphi,t)^*)\right]\right)(f) \\
&= \frac{1}{2}(\tilde{h}(\theta,\varphi,f) + \tilde{h}(\theta,\varphi,-f)^*) = \frac{1}{2}\left(\sum Y_{2,m}(\theta,\varphi)\tilde{h}^P_{2,m}(f) + \sum Y_{2,m}(\theta,\varphi)^*\tilde{h}^P_{2,m}(-f)^*\right) \\
&= \frac{1}{2}\sum S_{2,m}(\theta)\left[e^{im\varphi}\tilde{h}^P_{2,m}(f) + e^{-im\varphi}\tilde{h}^P_{2,m}(-f)^*\right] \\
&= \frac{1}{2}\sum S_{2,m}(\theta)\left[e^{im\varphi}e^{-i(2\epsilon+m\alpha)}d^2_{-2,m}(-\beta)\tilde{h}^{\rm D}_{2,-2}(f) + \left(e^{im\varphi}e^{i(2\epsilon-m\alpha)}d^2_{2,m}(-\beta)\tilde{h}^{\rm D}_{2,2}(-f)\right)^*\right] \\
&= \frac{1}{2}\sum S_{2,m}(\theta)A_D(f)e^{-i\phi_D(f)}\left[e^{im\varphi}e^{-i(2\epsilon+m\alpha)}d^2_{-2,m}(-\beta) + e^{-im\varphi}e^{-i(2\epsilon-m\alpha)}d^2_{2,m}(-\beta)\right] \qquad (16) \\
&= \frac{1}{2}A_D(f)e^{-i(\phi_D(f)+2\epsilon)}\sum S_{2,m}(\theta)\left[e^{im(\varphi-\alpha)}d^2_{-2,m}(-\beta) + e^{-im(\varphi-\alpha)}d^2_{2,m}(-\beta)\right] \qquad (17)
\end{aligned}$$

where the angles α, β and ϵ have to be evaluated at $\omega = \pi f$. We have written ${}^2Y_{l,m}(\theta,\phi) = S_{2,m}(\theta)e^{im\phi}$. For $h_\times$, one has

$$\begin{aligned}
\widetilde{h_\times}(\theta,\varphi,f) &= ({\rm FT}[-{\rm Im}\, h(\theta,\varphi,t)])(f) = \left({\rm FT}\left[\frac{i}{2}(h(\theta,\varphi,t) - h(\theta,\varphi,t)^*)\right]\right)(f) \\
&= \frac{i}{2}\sum S_{2,m}(\theta)A_D(f)e^{-i\phi_D(f)}\left[e^{im\varphi}e^{-i(2\epsilon+m\alpha)}d^2_{-2,m}(-\beta) - e^{-im\varphi}e^{-i(2\epsilon-m\alpha)}d^2_{2,m}(-\beta)\right] \qquad (18) \\
&= \frac{i}{2}A_D(f)e^{-i(\phi_D(f)+2\epsilon)}\sum S_{2,m}(\theta)\left[e^{im(\varphi-\alpha)}d^2_{-2,m}(-\beta) - e^{-im(\varphi-\alpha)}d^2_{2,m}(-\beta)\right] \qquad (19)
\end{aligned}$$

This is what is returned by ChooseFDWaveform. On these expressions, we can check that a (constant) shift $\alpha \to \alpha + \delta\alpha$ can be reabsorbed by a shift $\varphi \to \varphi + \delta\varphi$ with $\delta\alpha = \delta\varphi$ (as we already pointed out,

physically only the difference $\alpha - \phi$ is relevant). Furthermore, a shift $\epsilon \to \epsilon + \delta\epsilon$ can be reabsorbed by a shift in the coalescence phase of PhenomD $\phi_D \to \phi_D + \delta\phi$ since both parametrize a freedom of rotation in the orbital plane.

Also manifest from these expressions is the fact that under a shift $\epsilon \to \epsilon + \delta\epsilon$ (or equivalently of the coalescence phase of PhenomD since we just said they are degenerate), both waveforms transform as $h_{+,\times} \to e^{-2i\delta\epsilon} h_{+,\times}$. This trivial phase dependence (which is convenient for instance if one wants to analytically optimize a match over over this rotation freedom in the orbital plane) is a consequence of the fact that in the co-precessing we have only the $(\ell, |m|) = (2, 2)$ modes. This is similar to the aligned spin case where if one only considers the $(\ell, |m|) = (2, 2)$ the dependence of the full signal (any combination of the two polarizations) on the initial orbital phase (or coalescence phase etc...) in the frequency domain and when restricting to one side of the spectrum is a trivial multiplicative phase factor.

4 Outline of the derivation of closed form expressions for the angles

Notation: In this section, we follow the usual PN notation of e.g. [Class. Quant. Grav., 2013, 30, 075017]. In particular, we denote the Newtonian angular momentum (previously $\hat{\mathbf{L}}_\mathbf{N}$) as $\boldsymbol{\ell}$. The unit separation vector between the two bodies is denoted $\boldsymbol{n}$. A third vector $\boldsymbol{\lambda}$ is defined so that $\{\mathbf{n}, \boldsymbol{\lambda}, \boldsymbol{\ell}\}$ is an orthonormal triad.

To obtain closed form expressions for the Euler angles, we make the two following approximations

- We consider a single spin system (say $\mathbf{S}_1$=0), define some effective spin parameters (χ_ℓ, χ_p) from the components of $\mathbf{S}_2$ and derive expressions in terms of (χ_ℓ, χ_p). At the end, we also provide a mapping between double spin systems and (χ_ℓ, χ_p) and so that our single spin expressions can be used in the double spin case. The motivation for this mapping is provided in the paper, and (for χ_p) in [14].
- We use a post-Newtonian approximation (despite the fact that we will use our final expressions through merger). We use the framework developed in Blanchet et al [Phys.Rev., 2011, D84, 064041] and pushed to higher order in Marsat et al [Class.Quant.Grav., 2014, 31, 025023]. In particular, we restrict to spin-orbit interactions and we first focus on the precessional timescale where radiation reaction can be neglected and $\mathbf{J}$ can be considered as constant. At the very end, we will reintroduce radiation reaction through the variation of the orbital frequency, but we will still assume that the direction of $\mathbf{J}$ remains constant through the whole evolution.

If one only considers the spin-orbit effects in the dynamics, then

$$S_{2,\ell} = \mathbf{S_2} \cdot \boldsymbol{\ell} \equiv G m_2^2 \chi_\ell \tag{20}$$

is constant. Since the spins defined in PN are of conserved Euclidean norm, the magnitude of the projection on the orbital plane is also constant. We denote

$$S_2^\perp = \sqrt{S_{2,n}^2 + S_{2,\lambda}^2} \equiv G m_2^2 \chi_p. \tag{21}$$

which defines our effective spin χ_p. Note however that $S_{2,n} = \mathbf{S_2} \cdot \boldsymbol{n}$ and $S_{2,\lambda} = \mathbf{S_2} \cdot \boldsymbol{\lambda}$ individually are not constant. To leading order, they oscillate at a frequency given by the orbital frequency with corrections given by the precession frequency. This is because on timescales shorter than the precession timescale, the spin remains fixed in the inertial frame but the triad vectors move with the orbital frequency. In general, our expressions for the angles will depend on both $S_{2,n}$ and $S_{2,\lambda}$ and we will "average out" the oscillations over an orbit in order to obtain expressions that only depend on χ_p.

The main ingredient that we will need is the components of $\mathbf{J}$ in the triad $\{\mathbf{n}, \boldsymbol{\lambda}, \boldsymbol{\ell}\}$. These have been computed in the case of quasi-circular orbits (r constant up to radiation reaction effects) to next-to-next-to-leading-order (NNLO) in spin-orbit effects in Bohe et al. [Class. Quant. Grav., 2013, 30, 075017] (see eq (4.7)) in terms of the usual PN expansion parameter $x = \omega^{2/3}$ (formally of order $1/c^2$) and the component of the spins in the same triad. Note that J_ℓ only depends on the component of the spin that is orthogonal to the orbital plane, i.e. $S_{2,\ell}$ while J_n and J_λ depend on all three spin components. The leading order spin contribution to $\mathbf{J}$ appears at 0.5PN. The leading order of $\mathbf{J}$ is simply the Newtonian orbital angular momentum which is proportional to $\boldsymbol{\ell}$. Therefore, J_ℓ is of Newtonian order while J_λ and J_n are at least 0.5PN.

The opening angle β is the easiest to obtain as it is directly expressed in terms of the components of $\mathbf{J}$ under our approximation that $\hat{\mathbf{J}}$ remains constant throughout the evolution (remember that in principle β is the angle between $\boldsymbol{\ell}$ and $\hat{\mathbf{z}}$ which is only defined as $\hat{\mathbf{J}}$ *at* $f_{\rm ref}$).

$$\cos\beta = \boldsymbol{\ell} \cdot \frac{\mathbf{J}}{|\mathbf{J}|} = \frac{J_l}{\sqrt{J_\ell^2 + J_n^2 + J_\lambda^2}} \tag{22}$$

we can then PN reexpand the rhs (the leading order is 1...). Note that in doing so, we make the choice of keeping all the contributions non-linear in the spin that are generated (despite our original input being valid only to spin-orbit level; this is the same type of "arbitrary" choice that one makes when reexpanding the balance equation to define the various TaylorTx approximants). One can also invert this to obtain an expansion for β instead of $\cos\beta$ and then of any function of β.

The implementation of the model considers the spin angular momentum as $\mathbf{S} = \mathbf{S}_{||} + \mathbf{S}_{\perp}$, and the component of the total angular momentum parallel to the orbital angular momentum is $(L + S_{||})$, while the component in the orbital plane is only $S_{\perp}$. The cosine of the opening angle is then

$$\cos\beta = \frac{L + S_{||}}{\sqrt{(L + S_{||})^2 + S_{\perp}^2}} = \pm\left(1 + s^2\right)^{-1/2} \tag{23}$$

where $s = S_{\perp}/(L + S_{||})$ and where the sign depends on the sign of $L + S_{||}$. For small opening angles (which we expect for comparable mass ratios), we can approximate this as $\cos\beta \approx 1 - \frac{s^2}{2}$.... The most common appearance of this angle in the Wigner coefficients is $\cos(\beta/2)$, which can in turn be approximated as $\left(1 + \frac{s^2}{4}\right)^{-1/2}$ and a similar expression for the sine. This is what was used in version 1 of the code. Since the opening angle is in general *not* small, and since this expression already uses a computationally expensive square root, in IMRPhenomPv2 we use Eqn. (23) instead. We can write the cosine of the half-angle as

$$\cos(\beta/2) \quad = \quad \left(\frac{1 + \cos(\beta)}{2}\right)^{1/2} = \frac{1}{\sqrt{2}}\left(1 + (1 + s^2)^{-1/2}\right)^{1/2} \tag{24}$$

where we have chosen the positive sign in front of $(1+s^2)^{-1/2}$ regardless of the sign of $L+S_{||}$. The motivation for this is the following. In the aligned spin limit, the case where $(L + S_{||}) < 0$ corresponds to the final spin pointing in the opposite direction to the initial angular momentum, so the approximation that the direction of $\mathbf{J}$ remains fixed clearly breaks down. The code returns a warning in this situation as we don't control the accuracy of the model. However, the choice of a + sign at least ensures that the non precessing limit behaves as expected. Indeed, the role of β is to track the precession of $\hat{\mathbf{L}}_\mathbf{N}$ in the inertial frame aligned with *the initial* total angular momentum which only corresponds to the angle between $\hat{\mathbf{L}}_\mathbf{N}$ and $\hat{\mathbf{J}}$ if this last vector remains fixed. If instead it just flips direction (when $L + S_\ell$ changes sign in the aligned spin limit), the appropriate angle to describe the inclination of $\hat{\mathbf{L}}_\mathbf{N}$ in the inertial frame is now the angle between $\hat{\mathbf{L}}_\mathbf{N}$ and $-\mathbf{J}$,which corresponds to the + sign. Similarly,

$$\sin(\beta/2) = \frac{1}{\sqrt{2}}\left(1 - (1 + s^2)^{-1/2}\right)^{1/2}. \tag{25}$$

For the estimate of the orbital angular momentum, L, the original PhenomP implementation used the 2PN nonspinning expression from Eqs. (2.9) of Kidder (1995), with r/m taken from Eq. (4.13), and the 1PN approximation $v^2 = x = (M\omega)^{2/3}$. For the current version we use the standard 2PN nonspinning expression,

$$L_{\rm 2PN}(x, \eta) = \frac{\eta}{\sqrt{x}}\left(1 + \left(\frac{3}{2} + \frac{\eta}{6}\right)x + \left(3.373 - \frac{19\eta}{8} - \frac{\eta^2}{24}\right)x^2\right). \tag{26}$$

We then use the expression for $\dot{\alpha}$ derived in *Blanchet et al.* arXiv:1104.5659 (see (4.10a) combined with (4.8))

$$\frac{d\alpha}{dt} = -\frac{\omega_{\rm prec}}{\sin\beta}\frac{J_n}{\sqrt{J_n^2 + J_\lambda^2}} \tag{27}$$

where $\omega_{\rm prec}$ (which can be seen as a precession frequency for the orbital plane) is defined as $\dot{\boldsymbol{\ell}} = -\omega_{\rm prec}\boldsymbol{\lambda}$ and would vanish in the absence of spins in the orbital plane. The NNLO spin-orbit contribution for this quantity has been computed in [Class. Quant. Grav., 2013, 30, 075017] (there it is denoted ϖ; see (4.4) combined with the line below (4.1)). We re-expand the rhs and average over one orbit to get rid of the individual components $S_{2,n}$ and $S_{2,\ell}$ and obtain a function of χ_p (in addition to the masses and χ_ℓ). Similarly, using $\dot{\epsilon} = \dot{\alpha}\cos\beta$ we obtain an evolution equation for ϵ whose rhs is a PN expanded series depending only on ω, χ_ℓ and χ_p.

At this point, we reintroduce radiation reaction by allowing the orbital frequency to evolve and using it instead of time as the evolution parameter. We use the evolution equation $\dot{\omega}/\omega^2$ with corrections up to 3.5PN both in the non-spinning and the spin-orbit sector (which depend only on χ_ℓ). Upon rewriting

$$\frac{d\alpha}{d\omega} = \frac{1}{\dot{\omega}}\frac{d\alpha}{dt} \tag{28}$$

and PN reexpanding the rhs which is a series in ω whose coefficients are functions of the masses and the constant spin combinations χ_ℓ and χ_p, we can integrate term by term and obtain an explicit $\alpha(\omega)$ up to some integration constant α_0. We proceed in the same way for ϵ. Rather than reproducing these closed form

expressions here, we provide them in a Mathematica notebook available on the wiki at this *link*.

Note that our effective spin parameter χ_p only encodes the magnitude of the projection of the spin in the plane but that the orientation of the spin is to traced through α for single spin systems (α encodes the orientation of $\hat{\mathbf{L}}_\mathbf{N}$ but given the fact that $\mathbf{J} = \hat{\mathbf{z}}$ and given some value of ω, this uniquely fixes the spin for single spin systems). For double systems, the orientation of the individual spins is lost but α still provides the azimuthal angle $\hat{\mathbf{L}}_\mathbf{N}$The orientation of the spins in the orbital plane at $f_{\rm ref}$ that are passed by the user will be used to fix the integration constant α_0.

Having explained how we construct closed form expressions for the angles as a function of χ_p and χ_ℓ (the spin of the black hole), we need to provide a mapping between the six spin components provided by the user and χ_ℓ, χ_p. In the generic case of double spin systems, assuming $m_2 \geq m_1$, we define $Gm_1^2\chi_{1,\ell} = \boldsymbol{\ell} \cdot \mathbf{S}_1$ and $Gm2^2\chi_{2,\ell} = \boldsymbol{\ell} \cdot \mathbf{S}_2$, together with

$$\chi_p = \frac{\max_a \left[A_a |\mathbf{S}_a - (\boldsymbol{\ell} \cdot \mathbf{S}_a)\boldsymbol{\ell}|\right]}{A_2 m_2^2} = \frac{\max_a \left[A_a m_a^2 |\chi_{a,p}|\right]}{A_2 m_2^2} \tag{29}$$

where

$$A_a = 2 + \frac{3m_b}{2m_a}. \tag{30}$$

The motivation for the χ_p definition is given [14]. In the original v1 implementation of the model, both aligned spin components where combined into one single effective spin $\chi_{\rm eff} = (m_1\chi_1 + m_2\chi_2)/M$ and then we used the spin formulas with $\chi_\ell = \chi_{\rm eff}/m_2$ and $S_\ell = m_2^2\chi_\ell = m_2\chi_{\rm eff}$. When $\chi_{1,\ell} = 0$, this reduces to the correct single spin limit. However, since in IMPRPhenomPv2 we now use the two aligned spin components to feed the PhenomD underlying model, we also use them to construct

$$S_\ell = m_1^2\chi_{1,\ell} + m_2^2\chi_{2,\ell} \tag{31}$$

which provides a better estimate for the opening angle. For the other two angles, we simply use

$$\chi_\ell = \chi_{2,\ell}. \tag{32}$$

Note that Eq. (29) implies that depending on which black hole's in-plane spin dominates, we have that either $\chi_p = \chi_{2,p}$, or $\chi_p = W\chi_{1,p}$, where $W = \frac{3q+4}{4q^2+3q}$ and $q = m_2/m_1 \geq 1$. The weight function W is unity for equal masses and falls off as $1/q$ for large mass ratios. Consequently, the effective in-plane spin variable χ_p satisfies

$$\chi_p \leq \max\left[\chi_{2,p}, W(q)\chi_{1,p}\right], \qquad \chi_{2,p} \leq \sqrt{1-\chi_{2,\ell}^2}, \quad \chi_{1,p} \leq \sqrt{1-\chi_{1,\ell}^2}. \tag{33}$$

If the effective spin χ_p is taken as an independent variable, and not computed from the two individual black hole spins, it has to satisfy the above inequalities.

5 From the LAL frame to our inertial frame

In the `ChooseFDWaveform` interface, the user does not specify the configuration (direction of the spins and of $\hat{\mathbf{L}}_\mathbf{N}$...) at $f_{\rm ref}$ in the inertial frame depicted in Fig 1 and in which the model is naturally constructed. Rather, the interface refers to a different inertial frame where $\hat{\mathbf{z}}''$ coincides with $\hat{\mathbf{N}}$ and at $f_{\rm ref}$ the Newtonian orbital angular momentum LN is in the $x''z''$ plane (with positive projection on the x" axis).

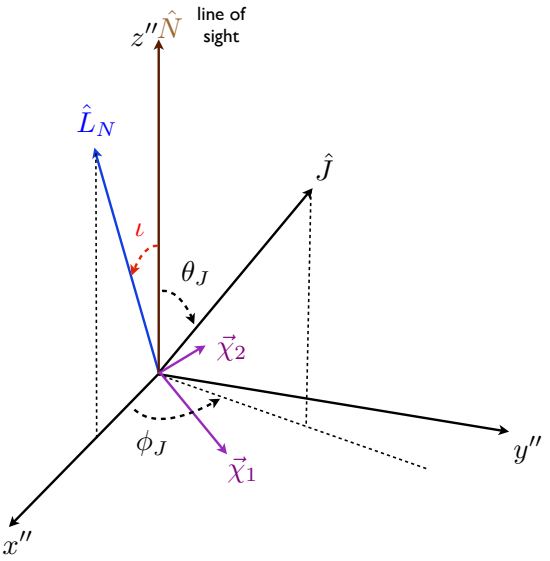

Figure 2: The frame in which the user specifies the configuration at $f_{\rm ref}$. Specifically, the user provides the inclination ι (i.e. the angle between $\hat{\mathbf{N}} = \hat{\mathbf{z}}''$ and $\hat{\mathbf{L}}_\mathbf{N}$, which together with the requirement that $\hat{\mathbf{L}}_\mathbf{N}$ is in the (x"z") plane fully determines $\hat{\mathbf{L}}_\mathbf{N}$) and the six spin components. From this, we reconstruct $\mathbf{J}$ (using a 2PN non-spinning approximation for the total orbital angular momentum $\mathbf{L}$ so that $\mathbf{L} = L_{2PN}\hat{\mathbf{L}}_\mathbf{N}$, and then $\mathbf{J} = \mathbf{L} + \mathbf{S}_1 + \mathbf{S}_2$), compute the spherical angles (θ_J, ϕ_J) and use those to rotate back to the frame of Fig 1 .

With the set of conventions currently used in LAL, the user specifies the 6 spin components in a frame adapted to $\hat{\mathbf{L}}_\mathbf{N}$ but these are rotated to the frame of Fig. 2 before being passed to the PhenomP function `CalculateModelParameters`.As described in the caption, we use them, together with a 2PN non spinning approximation to $\mathbf{L}$ to compute the components of $\mathbf{J}$ via

$$\mathbf{J} = \mathbf{L} + \mathbf{S}_1 + \mathbf{S}_2. \tag{34}$$

We then have

$$\theta_J = \arccos(J_{z''}/|J|) \tag{35}$$

and, using the function `atan2` to make sure that we pick the correct quadrant,

$$\phi_J = \texttt{atan2}(J_{y''}, J_{x''}). \tag{36}$$

When rotating to the frame of Fig 1, we have to make a choice since there the x and y axes had not been defined. We choose to put the line of sight in the xz plane and with a positive projection on x, so that $\varphi = 0$. With this choice, there is a unique rotation relating the two frames. The (passive) rotation matrix allowing us to express the components of any vector (say $\mathbf{u}$) in the inertial frame of Fig 1 starting from the components in the frame of Fig. 2 reads

$$\begin{pmatrix} u_x \\ u_y \\ u_z \end{pmatrix} = \begin{pmatrix} -\cos\theta_J\cos\phi_J & -\cos\theta_J\sin\phi_J & \sin\theta_J \\ \sin\phi_J & -\cos\phi_J & 0 \\ \sin\theta_J\cos\phi_J & \sin\theta_J\sin\phi_J & \cos\theta_J \end{pmatrix} \begin{pmatrix} u''_x \\ u''_y \\ u''_z \end{pmatrix}. \tag{37}$$

In the inertial frame of Fig 1, we now have $(\hat{J}_x, \hat{J}_y, \hat{J}_z) = (0, 0, 1)$ i.e. the z axis corresponds to the direction of the total angular momentum, $(\hat{N}_x, \hat{N}_y, \hat{N}_z) = (\sin\theta_J, 0, \cos\theta_J)$ i.e. the line of sight $\hat{\mathbf{N}}$ is in the xz plane, with positive projection on x

$$\theta = \theta_J, \quad \varphi = 0 \tag{38}$$

and finally the components of $\hat{\mathbf{L}}_\mathbf{N}$ at $f_{\rm ref}$

$$\begin{pmatrix} \hat{L}_{N,x} \\ \hat{L}_{N,y} \\ \hat{L}_{N,z} \end{pmatrix} = \begin{pmatrix} \cos\iota\sin\theta_J - \cos\theta_J\cos\phi_J\sin\iota \\ \sin\iota\sin\phi_J \\ \cos\theta_J\cos\iota + \cos\phi_J\sin\theta_J\sin\iota \end{pmatrix}. \tag{39}$$

From this, we can read

$$\alpha(f_{\rm ref}) = \texttt{atan2}(\hat{L}_{N,y}, \hat{L}_{N,x}). \tag{40}$$

Again, we highlight that although the evolution of α is expressed in terms of only one effective in plane spin parameter χ_p which encodes no information about the orientation of the spins in the plane, these orientations are used to determine the value $\alpha(f_{\rm ref})$.

Since $\epsilon(f_{\rm ref})$ is degenerate with the coalescence phase of PhenomD, we can make any arbitrary choice and we use $\epsilon(f_{\rm ref}) = 0$.

6 Merger remnant: final mass and final spin

The PhenomP construction of approximating a precessing waveform with a non-precessing one suggests that the radiated energy and thus the final mass will depend only weakly on precession. The final mass from precessing NR runs in the literature have been compared with the aligned spin formula in PhenomD, and good agreement has been found. For comparisons with NR, data have been used from the publicly available SXS catalog [9], and published results of the Georgia Tech [10] and RIT [15] groups, a total of 343 precessing simulations for which final state data were available. In the results shown below we have also used another 115 non-precessing results from these three data sets. The results are shown in Fig. 3. Maximal relative errors in the radiated energy reach almost 20%, however this happens for large mass ratios where little energy is radiated. The relative error of the final mass is below 0.5%. One can see that the non-precessing estimate systematically underestimates the radiated energy, which is possibly due to the fact that the precessing motion typically generates radiation in excess of corresponding non-precessing cases.

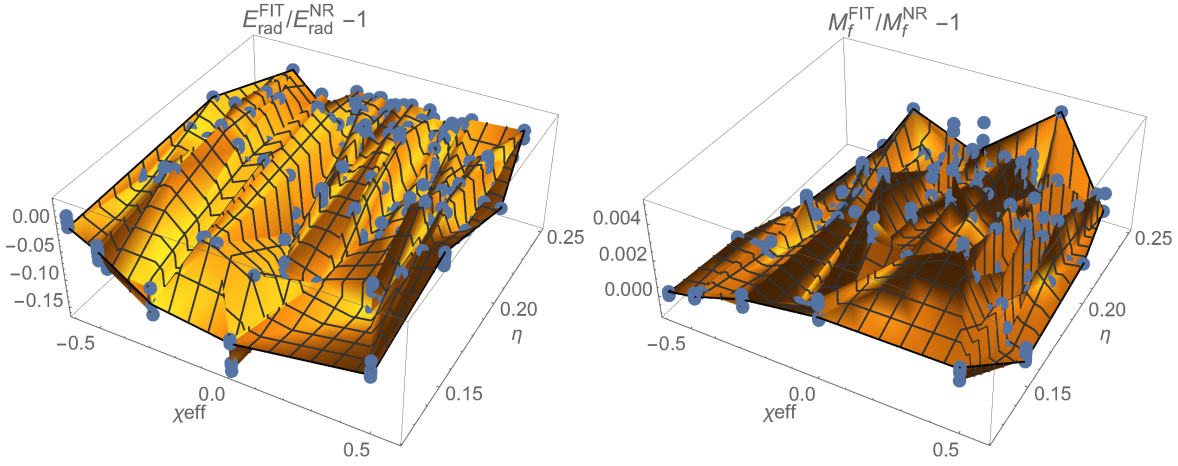

Figure 3: Relative errors between the PhenomD final mass formula (using the spin components projected unto the orbital angular momentum) and 343 precessing NR simulations: radiated energy (left) and final mass (right).

The final spin however does depend significantly on precession, as will be discussed below. PhenomP implementations `v1` and `v2` currently use the final mass estimate for the corresponding PhenomD waveform, and a simple estimate for the final spin magnitude, which takes into account precession effects based on similar assumptions as the approximate correspondence of precessing and non-precessing waveforms which underlies the PhenomP construction. PhenomPv1 directly uses the final spin formula developed in reference [11] (see also a derivation with rephrased assumptions in [4]), which we will refer to as the AEI spin formula. Below we outline how the final spin formula is motivated in reference [11], comment on the rephrasing of underlying assumptions in [4], construct similar final spin estimates which reduce to aligned spin formulas such as the one used in PhenomD, and compare them with data from precessing numerical relativity simulations.

The starting point of [11] is a fit to data from equal spin, unequal mass non-precessing NR simulations, where the final Kerr parameter a_{fin} is the projection of the dimensionless spin vector unto the normalized orbital angular momentum vector $\mathbf{L}/|\mathbf{L}|$) is computed as a function of the initial Kerr parameter a of both BHs (in the following we adapt notation to [11, 4]), and the symmetric mass ratio η as

$$a_{fin} = a + 2\sqrt{3}\eta + t_2\eta^2 + t_3\eta^3 + s_4 a^2\eta + s_5 a\eta^2 + t_0 a\eta, \tag{41}$$

with fitted coefficients $s_5 = -0.384, t_0 = -2.686, t_2 = -3.454, t_3 = 2.353$. The term $2\sqrt{3}\eta$ is motivated by the extreme mass ratio limit as discussed in[11]. This fit can be extended to an unequal spin, unequal mass fit by interpreting a as an effective spin parameter, in analogy to calibrating PhenomD to equal spin waveforms. Here, the appropriate effective spin parameter is defined as

$$\tilde{a} = \frac{m_1^2 a_1 + m_2^2 a_2}{m_1^2 + m_2^2} = \frac{a_1 + a_2 q^2}{1 + q^2}, \tag{42}$$

with the convention $q = m_2/m_1$ and $m_1 \geq m_2$, i.e. we substitute

$$a \;\rightarrow\; \tilde{a} \equiv \frac{a_1 + a_2 q^2}{1+q^2}\,, \tag{43}$$

and we have that

$$\tilde{a} \equiv a_{\rm tot}\frac{(1+q)^2}{1+q^2}\,, \tag{44}$$

with $a_{\rm tot} \equiv (a_1 + a_2 q^2)/(1+q)^2$ the total dimensionless spin.

In order to incorporate precession into the prediction, we can argue as follows: We can write the total angular momentum $\mathbf{J}$ as the sum of individual spins $\mathbf{S}_i$ and orbital angular momentum $\mathbf{L}$:

$$\mathbf{J} = \mathbf{S_1} + \mathbf{S_2} + \mathbf{L}.$$

In the PhenomP approximation, we assume that the total spin magnitudes, as well as the magnitudes of the projections of $\mathbf{S_1} + \mathbf{S_2}$ unto $\mathbf{L}$ ($S_{||}$) and orthogonal to it ($S_\perp$) are preserved, and that in a co-moving frame the waveform is well approximated by a twisted-up non-precessing waveform. Consequently, we can assume the magnitude of the precessing orbital angular momentum to be well approximated by the orbital angular momentum of the associated non-precessing configuration. As $|\mathbf{L}|$ decreases due to radiation reaction, the opening angle β increases, but $S_\perp$ and $S_{||}$ are assumed constant. If we assume that the radiation of angular momentum effectively stops at the "merger", and that the individual BH spin components relative to the direction of $\mathbf{L}$ are preserved up to the merger, then we can compute the final angular momentum as the vector-sum of 2 orthogonal components, and the magnitudes of the final spin S_{fin} and final Kerr parameter a_{fin} are given as

$$|S_{fin}| \equiv M_{fin}^2 |a_{fin}| = \sqrt{S_\perp^2 + (S_{||} + L_{fin})^2}.$$

Here, $S_\perp$ is the sum of the individual BH spins perpendicular to $\mathbf{L}$, and $S_{||}$ the sum of the individual BH spins parallel to $\mathbf{L}$, M_{fin} is the final mass, L_{fin} is defined by the equation

$$S_{||} + L_{fin} = M_{fin}^2 a_{fin}^{||},$$

and $a_{fin}^{||}$ is the final Kerr parameter in the corresponding non-precessing configuration.

We thus obtain the following estimate of the magnitude of the final precessing Kerr parameter:

$$|a_{fin}| = \sqrt{\left(S_\perp \frac{1}{M_{fin}^2}\right)^2 + {a_{fin}^{||}}^2}. \tag{45}$$

For later use, we introduce an alternative version, with a tuneable dimensionless parameter λ, which for consistency with our derivation would have to be set to unity:

$$|a_{fin}| = \sqrt{\left(S_\perp \frac{\lambda^2}{M_{fin}^2}\right)^2 + {a_{fin}^{||}}^2}, \tag{46}$$

Due to the change of the directions of $\mathbf{S}_i$ and $\mathbf{L}$ due to precession, this estimate only concerns the final spin magnitude and not its direction, and in the double spin case the result would depend on the time-dependent angle between the in-plane components of the spins. If we restrict to simple precession (total angular momentum not small compared to the orbital one and the spins), including the case that the waveform starts after a "flip of the direction of $\mathbf{J}$" in a case of transitional precession, we can assume that the direction of $\mathbf{J}$ is approximately preserved and agrees with the final spin direction.

Any prediction for the final spin of a non-precessing merger can be converted to an estimate for the final spin of a precessing merger using Eq. (46). The initial PhenomP implementation used the AEI final spin formula, Eq. (41) for a_{fin} in Eq. (46), plus two additional choices: First, the radiated energy is neglected, i.e. M_{fin} is assumed equal to the initial mass, which in Eq. (46) is equivalent to setting the parameter λ to $\lambda = M_{fin}/M_{in}$. Second, in Eq. (41) it would be natural to consider in Eq. (42) only spin components parallel to $\mathbf{L}$. In the AEI formula, however, this is only done for the terms linear in a, while the terms quadratic in a incorporate the entire BH spin including components in the orbital plane.

The AEI formula produces final spins in excess of the Kerr limit in some region of the parameter space as shown in Fig. 4, and also has not been calibrated to recent NR waveforms, thus an updated spin fit was developed for the PhenomD waveform model, and for PhenomPv2 we use a precessing final spin formula which reduces to the PhenomD value in the aligned spin case. Two alternative versions of Eq. (46) have been considered, where $a_{fin}^{||}$ is computed by the fit used in PhenomD, and the parameter λ is either set to unity or to M_{fin}^2.

The AEI final spin estimate is implemented in the IMRPhenomP LAL code corresponding to the equations in [11]. There, a quantity $\boldsymbol{\ell}$ is defined via

$$\boldsymbol{a}_{\rm fin} = \frac{1}{(1+q)^2}\left(\boldsymbol{a}_1 + \boldsymbol{a}_2 q^2 + \boldsymbol{\ell} q\right)\,, \tag{47}$$

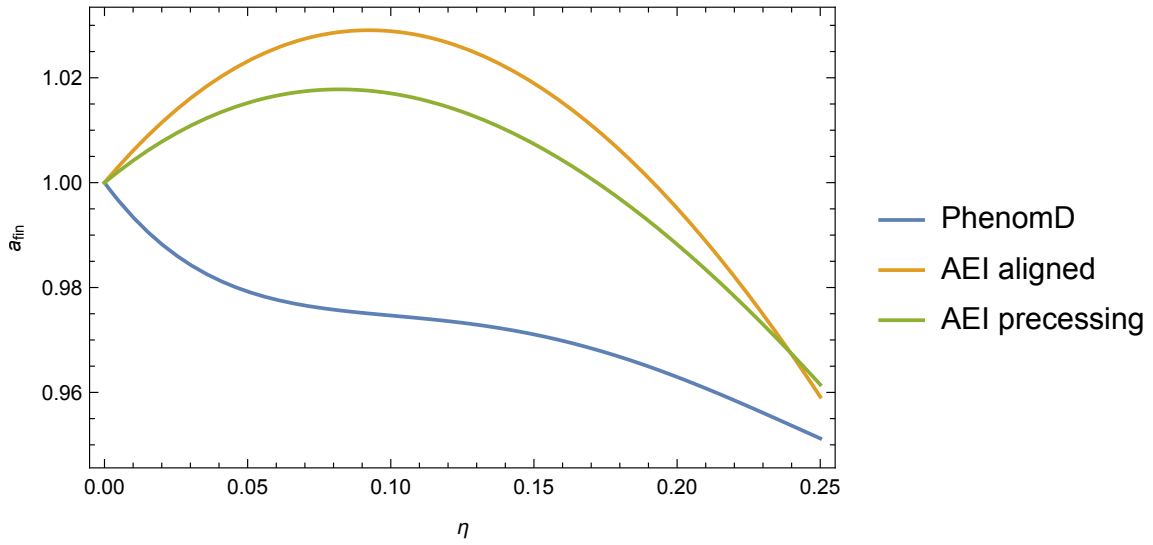

Figure 4: Comparison of final spin fits for non-precessing extreme Kerr black holes as a function of symmetric mass ratio. The PhenomD fit respects the Kerr limit. The AEI non-precessing fit, and its precessing generalization (which does not agree with the original non-precessing fit in the non-precessing case) both violate the Kerr limit.

the norm of the final spin then reads

$$|\boldsymbol{a}_{\rm fin}| = \frac{1}{(1+q)^2}\Big[|\boldsymbol{a}_1|^2 + |\boldsymbol{a}_2|^2 q^4 + 2|\boldsymbol{a}_2||\boldsymbol{a}_1| q^2 \cos\alpha + 2\left(|\boldsymbol{a}_1|\cos\beta + |\boldsymbol{a}_2| q^2 \cos\gamma\right)|\boldsymbol{\ell}| q + |\boldsymbol{\ell}|^2 q^2\Big]^{1/2}, \tag{48}$$

where the three (cosine) angles α, β and γ (we use the same notation as [11], note that these quantities are not the same as other quantities of the same name used in other sections) are defined by

$$\cos\alpha \equiv \hat{\boldsymbol{a}}_1 \cdot \hat{\boldsymbol{a}}_2\,, \quad \cos\beta \equiv \hat{\boldsymbol{a}}_1 \cdot \hat{\boldsymbol{\ell}}\,, \quad \cos\gamma \equiv \hat{\boldsymbol{a}}_2 \cdot \hat{\boldsymbol{\ell}}\,. \tag{49}$$

The quantity $\boldsymbol{\ell}$ is computed as

$$|\boldsymbol{\ell}| = \frac{s_4}{(1+q^2)^2}\left(|\boldsymbol{a}_1|^2 + |\boldsymbol{a}_2|^2 q^4 + 2|\boldsymbol{a}_1||\boldsymbol{a}_2| q^2 \cos\alpha\right) + \left(\frac{s_5\nu + t_0 + 2}{1+q^2}\right)\left(|\boldsymbol{a}_1|\cos\beta + |\boldsymbol{a}_2| q^2 \cos\gamma\right) + 2\sqrt{3} + t_2\nu + t_3\nu^2\,, \tag{50}$$

which follows from Eqs. (48)-(50), and as discussed above uses the complete BH spins in the term quadratic in spins, and the components in the direction of $\mathbf{L}$ in the linear spin term.

An ambiguity exists of how the PhenomP effective spin parameters χ_{eff} and χ_p are mapped to the input for the final spin formula. The current IMRPhenomPv2 implementation uses a function

`FinalSpinIMRPhenomD_all_in_plane_spin_on_larger_BH`,

which chooses the spin vectors as

$$\mathbf{a}_1 = \{\chi_p, 0, \chi_{1l}\}, \qquad \mathbf{a}_2 = \{0, 0, \chi_{2l}\}. \tag{51}$$

In Fig. 5 we compare five versions of final spin estimates: the original AEI formula [11], the expression implemented for PhenomPv2, which uses Eq. (46) combined with Eq. (51) and $\lambda = M_{fin}/M_{ini}$, the same but with $\lambda = 1$, an alternative 'improved" PhenomP version not using Eq. (51), i.e. we track the contributions of the two BHs to the in-plane spin ("PhenomP+"), and the same using an unpublished non-precessing final spin fit which takes into account unequal spin effects ("PhenomP++"). Figure 5 shows both the sorted residuals from 350 precessing simulations, and from non-precessing SXS simulations. One can see that for non-precessing simulations, PhenomD is significantly more accurate than the AEI fit, and further accuracy can be gained by taking into account unequal spin effects. Note that the discrepancies in accuracy would be much larger, if we had available unequal mass simulations with very large spins.

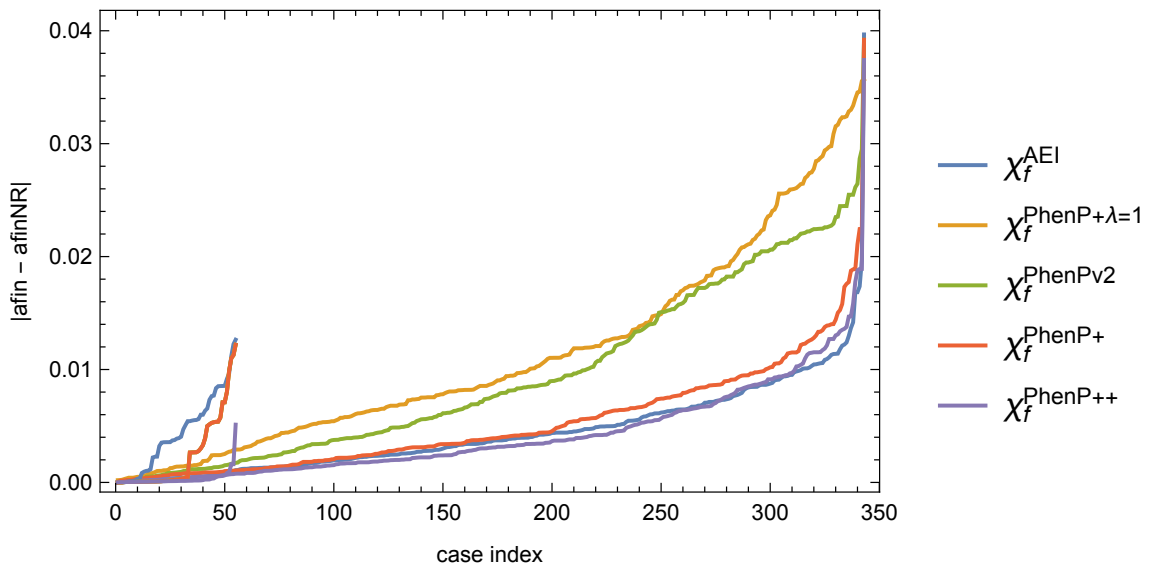

Figure 5: Residuals for the final spin magnitude for 3 different formulas described in the text, relative to 343 NR data sets.

RMS errors for comparing to 343 precessing NR cases are 0.013 for using the PhenomD final spin in Eq. (46) with $\lambda = 1$, 0.0064 for doing the same with $\lambda = M_{fin}$, 0.0056 for the AEI final spin formula, 0.0067 for the PhenomP+ version, and 0.0052 for the PhenomP++ version. The largest errors for our set of precessing cases are thus obtained for the PhenomD version of $a_{fin}^{||}$ and $\lambda = 1$. Note that Fig. 4 implies that a large number of cases with a large spin component in the direction of the orbital angular momentum and correspondigly little precession would lead to large errors of the AEI fit for such a data set. The remaining RMS error is probably mostly due to the neglecting the detailed merger physics in this simple approach. Our comparison suggests a straightforward generalization of the PhenomPv2 final spin formula to double spin systems, where we track all spin components for the final spin calculations, as in our PhenomP+ and PhenomP++ versions.

In addition, relative errors in the final spin are plotted in Fig. 6 versus effective spin in the direction of the orbital angular momentum, χ_{eff}, η, χ_p and maximal $\cos\beta$ computed from Eq. 26. As can be seen in the plot, there are no clear correlations. The most extreme values of s are ≈ 4.5 and ≈ -182. The latter correspond to the most extreme value of β, of ≈ 90.3 degrees, corresponding to six cases from the RIT data set, at mass ratio 6, with the smaller black hole nonspinning, and the spin of the larger black hole, $\chi_1 = 0.8$, inclined at 150 degrees with respect to the orbital angular momentum. The angle between the initial and final angular momentum is about 20 degrees, and the error in the predicted magnitude of the final spin is about 2.5%.

7 Faithfulness

7.1 Summary of the method

For a given configuration, we rotate the NR waveform to the frame where initially J is z. The waveform seen by a detector in the direction (θ, ϕ) depends on its orientation parametrize by the 3 angles (two angles for the direction of the source in the detector's sky and a polarization angle) which enter the antenna patterns. Because our match computations optimize over amplitude, these 3 angles reduce to one parameter κ).

For a given choice (θ, ϕ, κ) for the NR signal, we compute the match against the model and optimize over time of coalescence, initial orbital phase of the binary in the orbital plane (ϵ_0), initial orientation of $\mathbf{L}_N$ around $\mathbf{J}$ (i.e. α_0) and polarization. The other parameters are set to the NR values. This is very similar to what is done in SEOBNRv3.

Then, we average over the NR angles (ϕ, κ). The distribution for κ is the one corresponding to "uniform" orientations of the detector and for ϕ we take uniform in $[0, 2\pi]$. Therefore, for each "inclination" θ of the NR signal we obtain one number which we call faithfulness. For the SEOBNRv3 review, a very similar procedure was used, except that a fixed value for ϕ was chosen (instead of averaging over this angle).

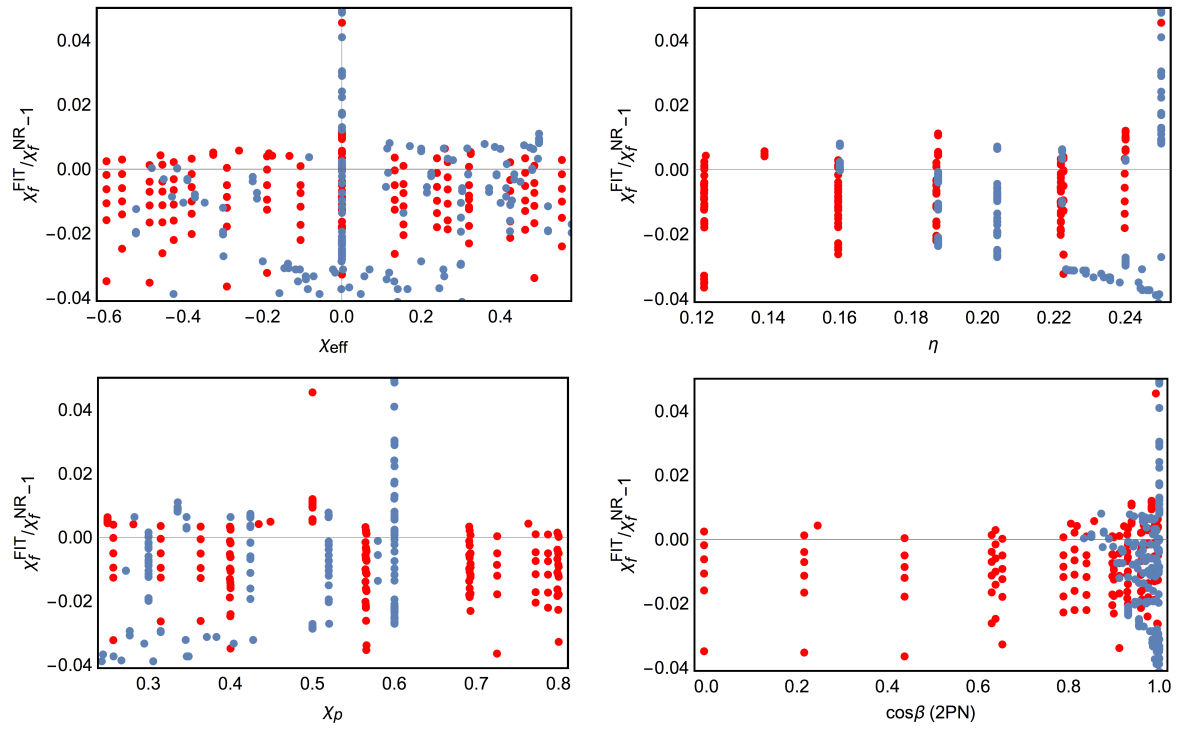

Figure 6: Relative errors for the final spin magnitude, relative to 343 NR data sets, plotted versus effective spin in the direction of the orbital angular momentum, χ_{eff}, η, χ_p and $\cos\beta$. Red dots mark single spin cases, blue dots double spin cases.

7.2 Results

NR waveforms: from SXS catalog, a set of 32 wfs ("Random 32") with mass ratios in [1,2]. Also sets of precessing waveforms with q=1.5, 3 and 5. This is the same set of waveforms that was used in the SEOBNRv3 review.

We choose several representative inclinations $\pi/12$ (close to "face on"; note that the inclination changes during the evolution because of precession and this is defined at the beginning of the NR simulation. But since we define inclination as the angle between the total angular momentum **J** and the line of sight, this doesn't change much during the evolution for simple precession), $\pi/2$ (edge on) and the intermediate value $\pi/3$. As one goes from the face on to the edge on case, the modulations due to precession become more important and the unfaithfulness increases.

7.2.1 Close to face-on orientation

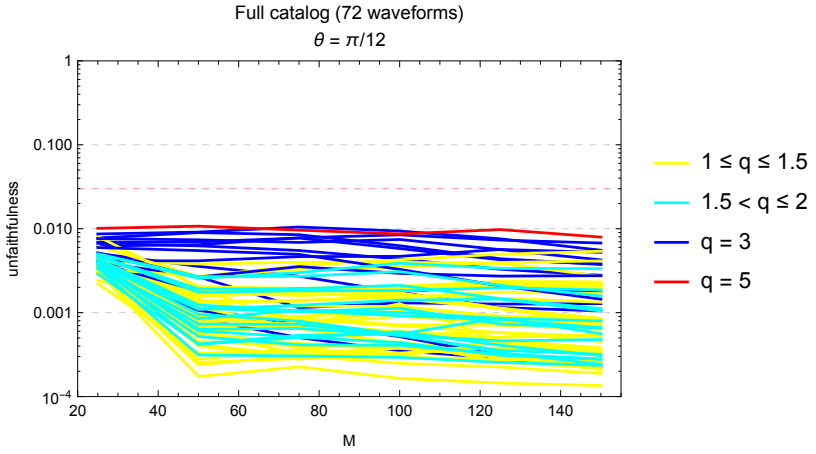

Figure 7: Close to face-on orientation. Red dashed line is 3%.

7.2.2 Intermediate orientation

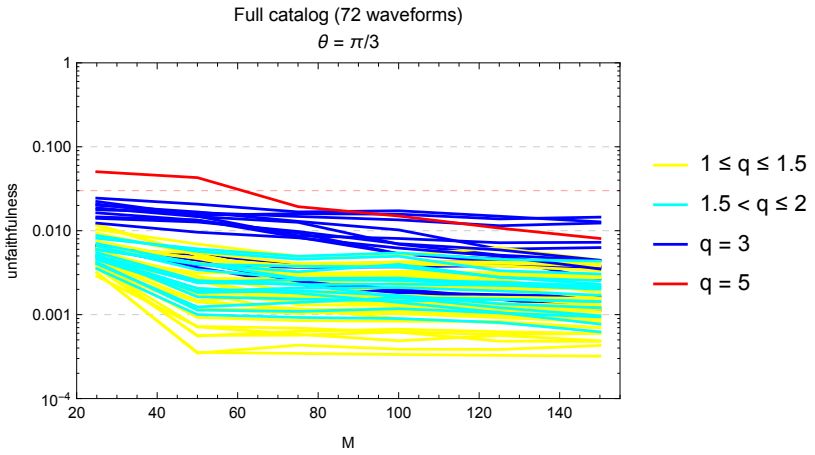

Figure 8: Intermediate orientation. Red dashed line is 3%.

7.2.3 Close to edge-on orientations

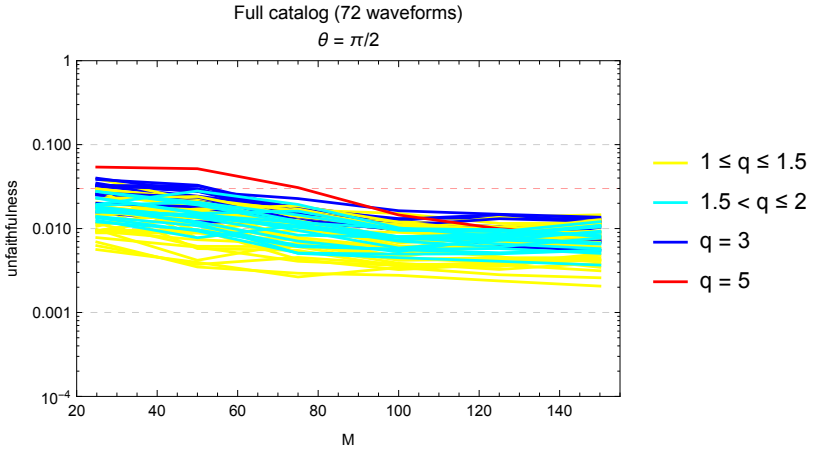

Figure 9: Close to edge-on orientation. Red dashed line is 3%.

8 Contours of max opening angle: an indication of where the model accuracy degrades

The accuracy of the model is expected to degrade as the opening angle β increases (precession becomes stronger) and investigating the domain of validity of the small opening angle approximation can provide some guidance in determining the region of parameter space where the model is accurate. One should however keep in mind that first, we have no way of quantifying how the performance of the model correlates with the value of the opening angle and second, that several other approximations are also made in the model whose domain of validity are not investigated here (e.g. the fact that $\mathbf{J}$ remains approximately fixed in direction, the fact that we neglect $\ell > 2$ harmonics, the fact that we approximate precession via this twisting procedure of aligned spin waveforms, the SPA pushed through merger, the effective precessing spin ...). Note that other models also share some of these approximations. Ultimately, only comparisons with NR can tell us where the model is and isn't accurate. We have done these comparisons for the currently available NR waveforms (see faithfulness plots) but these cover a small portion of parameter space. [In fact, the one with the largest opening angle that we have is the $q = 5, \chi_p = 0, \chi_{1,\ell} = \chi_{2,\ell} = 0$ is barely above $\pi/5$].

- Let's determine the region of parameter space for which $\beta < \beta_{\rm threshold}$.
- The expression for $\cos\beta$ is given in Section III. It is

$$\cos\beta = \left(1 + s^2\right)^{-1/2} \tag{52}$$

where s can be rewritten (assuming $m_1 > m_2$) as

$$s = S_\perp/(L + S_{||}) = \frac{(q/(1+q))^2 \chi_p}{L_{2PN}[q, Mf] + (q^2\chi_{1,\ell} + \chi_{2,\ell})/(1+q)^2)} \tag{53}$$

i.e. it depends depends on $q, \chi_{1,\ell}, \chi_{2,\ell}, \chi_p$ and the combination Mf. For all values of q, the function $L_{2PN}(f)$ decreases at low frequencies then reaches a minimum and starts increasing again.

- For sufficiently negative aligned spin projections $\chi_{a,\ell}$ and sufficiently high mass ratio, the denominator in (53) can become negative during the evolution (in the aligned spin limit, this corresponds to **J** flipping, see discussion below (24)). For those cases, the evolution of $\cos\beta$ according to our formula is to decrease until the denominator vanishes (at which point we have $\cos\beta = 0$ i.e. $\beta = \pi/2$) and then to grow again (i.e. β decreases), due to our choice of + sign in (24). As discussed there, these are cases where we don't control the behavior of the model and these cases are flagged in the code (a warning is issued). Note however that in the exactly aligned case ($\chi_p = 0$) the waveform exactly reproduces PhenomD so these cases are fine and not flagged[1].
- From now on, we restrict to configurations for which the denominator remains positive throughout the evolution. This means we consider thresholds $\beta_{\text{threshold}}$ larger than $\pi/2$. The angle β starts infinitely small in the remote past (because L tends to infinity in the past) then grows during the inspiral up to a maximum close to merger after which it starts decreasing again. This is the behavior observed in NR simulations and well reproduced by our model thanks to the fact that $L_{2PN}(Mf)$ also reaches a minimum as f increases. See an example below

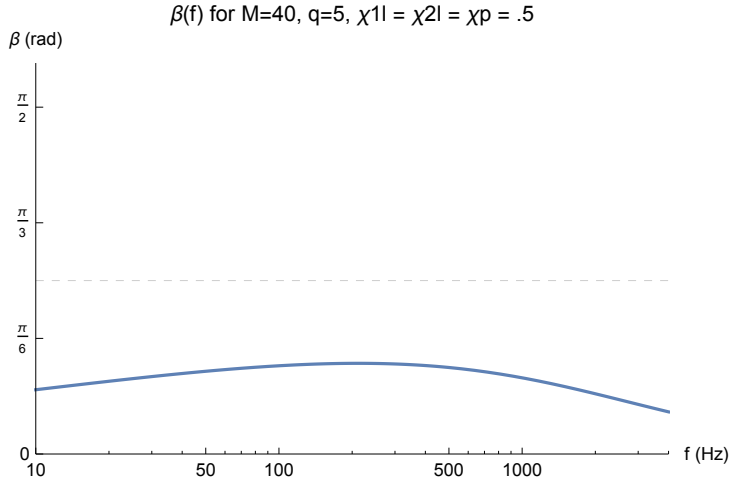

Figure 10: Typical frequency evolution of the opening angle.

- Let's impose that $\beta < \beta_{\text{threshold}}$ throughout the whole coalescence. For this we just need that

$$\max_{(Mf)} \beta < \beta_{\text{threshold}} \tag{54}$$

This max is reached when L_{2PN} reaches its minimum, which can be determined analytically since we use this very simple 2PN approximation for L. We have

$$(Mf)_{\max} = \frac{1}{\pi}\left(\frac{2\left(-\sqrt{-17\nu^2 - 1008\nu + 1539} + \nu + 9\right)}{3\left(\nu^2 + 57\nu - 81\right)}\right)^{2/3} \tag{55}$$

In fact, we could impose a weaker condition, namely that $\beta < \beta_{\text{threshold}}$ needs to be satisfied only for frequencies accessible to the detectors: the opening angle only reaches its maximum very close to merger and for low mass systems, this maximum could be out of band and the largest opening angle in band could be much smaller. This however introduces a dependence on the mass and for the sake of simplicity, we stick to $\max_{(Mf)} \beta < \beta_{\text{threshold}}$ regardless of whether the max is reached. Just for information, let's still plot below the frequency at which the max is reached as a function of M.

[1]The accuracy of the model may still be reasonable (in terms of matches for instance) around this exactly aligned limit: for small non-zero χ_p, $\cos\beta$ is always ~ 1 except in a small region (whose width is controlled by χ_p) around the frequency where the denominator vanishes in which $\cos\beta$ drops to 0 and then goes back to 1. This has not been investigated further and the warning is issued no matter how small χ_p is as long as it is not 0.

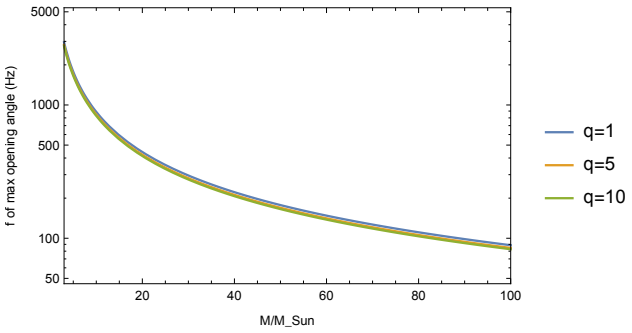

Figure 11: Frequency at which the maximum opening angle is reached. The dependence on q is extremely weak. For low mass systems, the maximum happens out of band and we could have imposed a weaker condition than the maximum being smaller than $\beta_{\rm threshold}$. For the sake of simplicity, we don't do this.

- We are left with a dependence on $q, \chi_{1,\ell}, \chi_{2,\ell}, \chi_p$ which is still too much for plotting contours and is anyway an unpractical set of variables in which to formulate a domain of validity. We therefore impose the additional condition that for a given set of $(q, \chi_{1,\ell}, \chi_{2,\ell})$ the opening angle remains smaller than the desired threshold for all possible values of χ_p. Since the opening angle increases with χ_p, we just need to impose that this condition is satisfied for the max χ_p that can be obtained given $(q, \chi_{1,\ell}, \chi_{2,\ell})$, which is

$$\chi_{p,\rm max} = \frac{\max\left(A_1 m_1^2 \sqrt{1-\chi_{1,\ell}^2}, A_2 m_2^2 \sqrt{1-\chi_{2,\ell}^2}\right)}{m_1^2 A_1} \tag{56}$$

  where the A_a have been defined in (30).
- We can now draw contours in the $(\chi_{1,\ell}, \chi_{2,\ell})$ plane for given values of the mass ratio q.

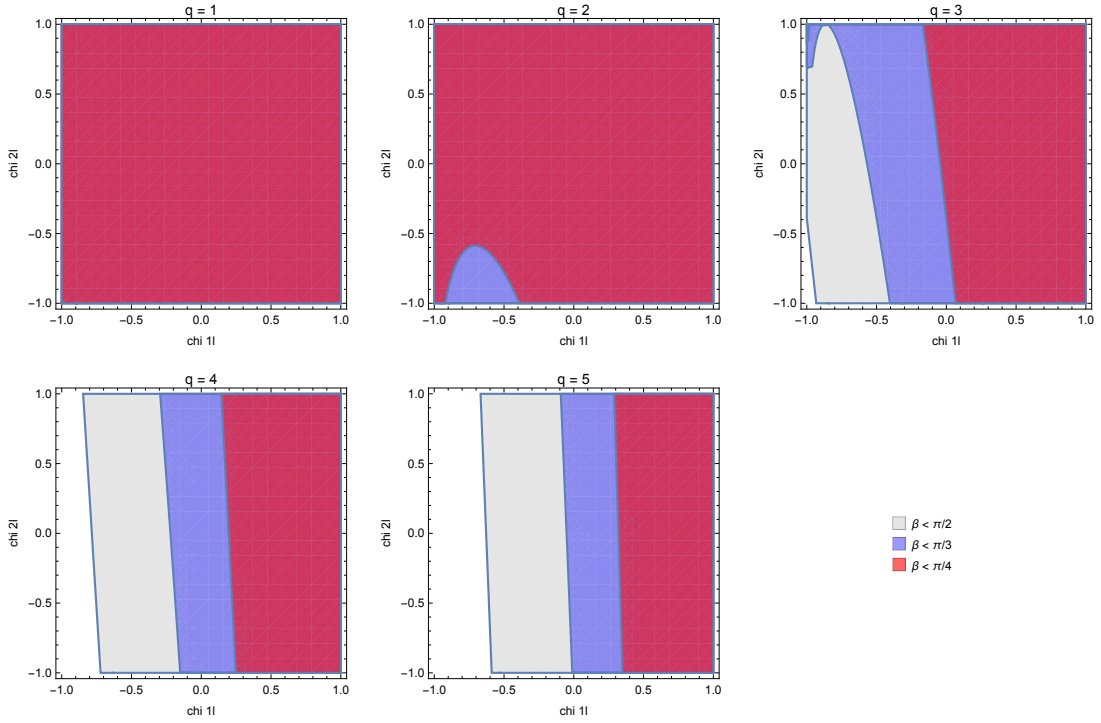

Figure 12: Contours in the $(\chi_{1,\ell}, \chi_{2,\ell})$ plane for fixed values of q for which the opening angle β remains larger than several thresholds for all values of χ_p and throughout the frequency evolution. As we move to more anti aligned spins, the opening angle increases. As the mass ratio increases, the contour is mostly determined by the spin of the largest BH. The non trivial shape of the contours for comparable masses for large anti aligned spins comes from the interplay between the fact that S_ℓ becomes more negative (which makes β larger) and the fact that as one moves into this region, the largest values of χ_p that are allowed become smaller. One should however keep in mind that the color at each (q, χ_1, χ_2) on these plots is determined by the maximal χ_p but that for smaller χ_p the opening angle is smaller (and goes to zero in the aligned spin limit).

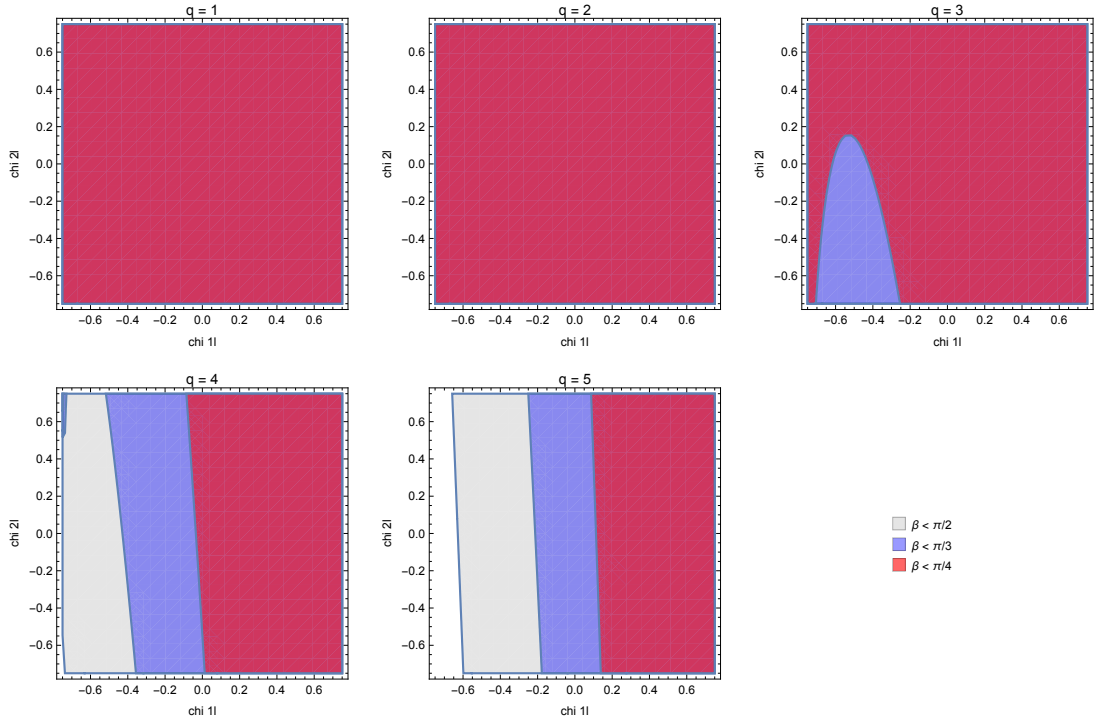

Figure 13: Same as above but with spin magnitudes limited to $|\chi_1|, |\chi_2| < 0.75$

- In practice, the code issues a warning
  - if $L_{2PN} + S_{1,\ell} + S_{2,\ell} < 0$ at the frequency where L_{2PN} reaches its minimum (computed from (55)).
  - if $\max \beta$ computed using Eqs.(52),(53) and (55) is larger than $\pi/4$ since we cannot test the accuracy of the model against NR waveforms in this regime.
- As an illustration of how the unfaithfulness correlates with the max opening angle (at least in the region where we have NR waveforms to test this), we reproduce the plots in Sec. 7.2 but instead of coloring the curves by mass ratio, we color them by max β as computed from Eqs.(52),(53) and (55) (we do not extract the actual opening angle from the NR data)).

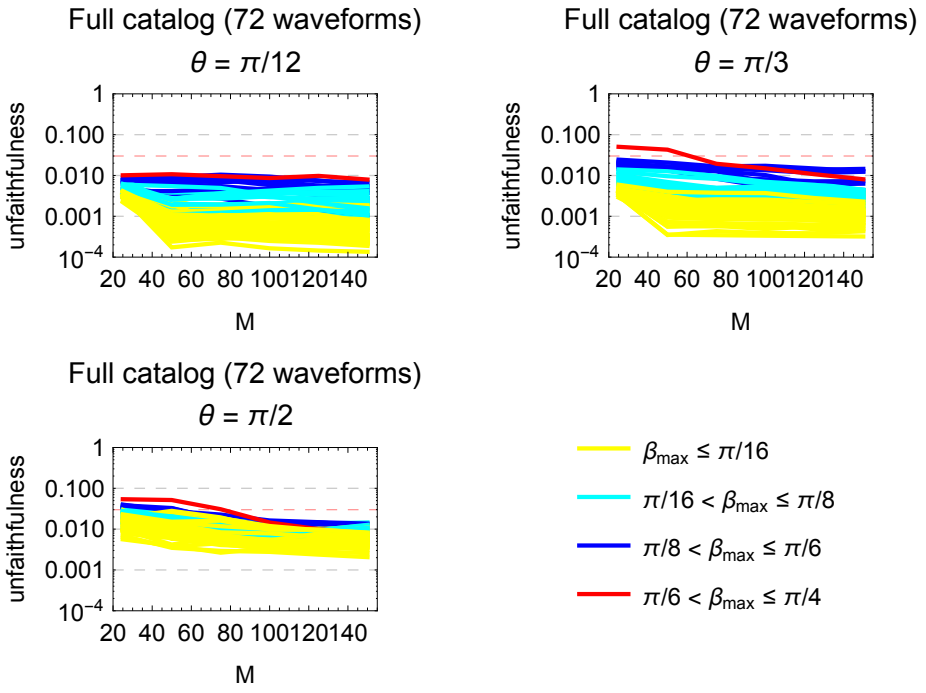

Figure 14: Same plots as in Sec. 7.2 but colored by $\max\beta$ instead of q. The largest value (red curve) is $\max\beta \simeq 0.21\pi \simeq \pi/5$.

References

[1] `https://www.lsc-group.phys.uwm.edu/ligovirgo/cbcnote/WaveformsReview/IMRPhenomPv2CodeReview`.

[2] `https://www.lsc-group.phys.uwm.edu/ligovirgo/cbcnote/WaveformsReview/IMRPhenomDCodeReview`.

[3] K. G. Arun, Alessandra Buonanno, Guillaume Faye, and Evan Ochsner. Higher-order spin effects in the amplitude and phase of gravitational waveforms emitted by inspiraling compact binaries: Ready-to-use gravitational waveforms. *Phys. Rev.*, D79:104023, 2009. [Erratum: Phys. Rev.D84,049901(2011)].

[4] Enrico Barausse and Luciano Rezzolla. Predicting the direction of the final spin from the coalescence of two black holes. *Astrophys. J.*, 704:L40–L44, 2009.

[5] Michael Boyle, Robert Owen, and Harald P. Pfeiffer. A geometric approach to the precession of compact binaries. *Phys. Rev.*, D84:124011, 2011.

[6] Mark Hannam, Patricia Schmidt, Alejandro Bohé, Leïla Haegel, Sascha Husa, Frank Ohme, Geraint Pratten, and Michael Pürrer. Simple Model of Complete Precessing Black-Hole-Binary Gravitational Waveforms. *Phys. Rev. Lett.*, 113(15):151101, 2014.

[7] Sascha Husa, Sebastian Khan, Mark Hannam, Michael Pürrer, Frank Ohme, Xisco Jiménez Forteza, and Alejandro Bohé. Frequency-domain gravitational waves from non-precessing black-hole binaries. I. New numerical waveforms and anatomy of the signal. 2015.

[8] Sebastian Khan, Sascha Husa, Mark Hannam, Frank Ohme, Michael Pürrer, Xisco Jiménez Forteza, and Alejandro Bohé. Frequency-domain gravitational waves from non-precessing black-hole binaries. II. A phenomenological model for the advanced detector era. 2015.

[9] Abdul H. Mroue et al. Catalog of 174 Binary Black Hole Simulations for Gravitational Wave Astronomy. *Phys. Rev. Lett.*, 111(24):241104, 2013.

[10] L. Pekowsky, R. O'Shaughnessy, J. Healy, and D. Shoemaker. Comparing gravitational waves from nonprecessing and precessing black hole binaries in the corotating frame. *Phys. Rev.*, D88(2):024040, 2013.

[11] Luciano Rezzolla, Enrico Barausse, Ernst Nils Dorband, Denis Pollney, Christian Reisswig, Jennifer Seiler, and Sascha Husa. On the final spin from the coalescence of two black holes. *Phys. Rev.*, D78:044002, 2008.

[12] Patricia Schmidt, Mark Hannam, and Sascha Husa. Towards models of gravitational waveforms from generic binaries: A simple approximate mapping between precessing and non-precessing inspiral signals. *Phys. Rev.*, D86:104063, 2012.

[13] Patricia Schmidt, Mark Hannam, Sascha Husa, and P. Ajith. Tracking the precession of compact binaries from their gravitational-wave signal. *Phys. Rev.*, D84:024046, 2011.

[14] Patricia Schmidt, Frank Ohme, and Mark Hannam. Towards models of gravitational waveforms from generic binaries II: Modelling precession effects with a single effective precession parameter. *Phys. Rev.*, D91(2):024043, 2015.

[15] Yosef Zlochower and Carlos O. Lousto. Modeling the remnant mass, spin, and recoil from unequal-mass, precessing black-hole binaries: The Intermediate Mass Ratio Regime. *Phys. Rev.*, D92(2):024022, 2015.